Crystallization Behavior of Poly(L-lactic acid)/ Montmorillonite Nanocomposites

Su-Mei Huang,[1] Jiunn-Jer Hwang,[1] Hsin-Jiant Liu,[2] Li-Huei Lin[2]

[1]*Department of Chemical Engineering, Army Academy, Chung-Li 320, Taiwan, Republic of China*
[2]*Department of Chemical and Materials Engineering, Vanung University, Chung-Li 320, Taiwan, Republic of China*

Received 29 September 2008; accepted 13 December 2009
DOI 10.1002/app.31966
Published online 17 March 2010 in Wiley InterScience (www.interscience.wiley.com).

ABSTRACT: In this study, we modified montmorillonite (MMT) with dilauryl dimethyl ammonium bromide (DDAB) and then exfoliated the structures in a poly(L-lactic acid) (PLLA) matrix. We used polar optical microscopy and X-ray diffraction (XRD) to examine the morphologies of the resulting composites, differential scanning calorimetry to study the melting and crystallization behavior, and Fourier transform infrared (FTIR) and Raman spectroscopy to measure the influence of the intermolecular interactions between PLLA and MMT on the isothermal crystallization temperature. We found that the DDAB-modified MMT was distributed uniformly in the PLLA matrix. At temperatures ranging from 130 to 140°C, the crystalline morphology resembled smaller Maltese cross-patterned crystallites; at temperatures from 150 to 170°C, however, the number of crystallites decreased, their sizes increased, and they possessed ringed spherulite structures. In the XRD spectra, the intensity of the diffraction peaks of the 200/110 and 203 facets of the PLLA/MMT nanocomposites decreased as the crystallization temperature increased. In the FTIR spectra, the absorption peak of the C=O groups split into two signals at 1748 and 1755 cm^{-1} when the isothermal crystallization temperature was higher than 140°C. © 2010 Wiley Periodicals, Inc. J Appl Polym Sci 117: 434–442, 2010

Key words: clay; crystallization; nanocomposites

INTRODUCTION

Poly(lactic acid) (PLA) is a linear aliphatic thermoplastic polyester that is considered to be a green polymeric material. It is the most commonly employed bioresorbable, biodegradable,[1] and biocompatible polymer. Microbial action (e.g., by bacteria or fungi) can decompose PLA into carbon dioxide and water and leave no hazardous residues. The versatility of PLA enables its extensive application in every field of conventional plastic processing. Products incorporating PLA are encountered commonly in daily life and in biomedical applications (e.g., sutures, bioresorbable bones, nails, and plates, carriers for drug release, and scaffolds for tissue engineering).

The properties of PLA depend on its molecular weight, molecular weight distribution, and purity and the process used for its manufacture. These data, however, are not always available in the literature or are very rare. Poly(L-lactic acid) (PLLA) is a semicrystalline polymer (its crystallinity can be greater than 40%) having a melting point (T_m) ranging from 170 to 200°C and a glass-transition temperature (T_g) ranging from 55 to 65°C. Poly(DL-lactic acid) (PDLLA) is an amorphous polymer having values of T_g ranging from 50 to 60°C with an undetectable value of T_m. Although PLLA is soluble only in chloroform and dichloromethane, PDLLA can be dissolved in most organic solvents [e.g., tetrahydrofuran (THF), acetone, chloroform, and benzene]. Because of the presence of its methyl side groups, PLA is less hydrophilic than polyglycolide and degrades more slowly. In fact, the degradation of PLA can take up to 2 years; this depends on the initial molecular weight, morphology, stereochemistry, and dimensions of the polymeric material.

Montmorillonite (MMT) is a highly rigid, flaky substance. After the addition of MMT to a polymeric matrix, the mobility of the molecular chains is suppressed, and this improves the dimensional stability, thermal stability, and mechanical properties of the polymer. Surface-treated, inorganic, laminar MMT has been introduced into several polymer matrices, including polyurethane, poly(methyl methacrylate)/poly(styrene-*co*-acrylonitrile), nylon 6, epoxy resin, and polyimide, to improve their thermal stability, mechanical strength, flame retardancy, or gas permeability.[2–12] Polymer/MMT nanocomposites can be prepared through exfoliation or intercalation of MMT in the polymer matrix with various methods, such as intercalation of the polymer or prepolymer

Correspondence to: J.-J. Hwang (jiunnjer1@hotmail.com).
Contract grant sponsor: National Science Council of the Republic of China; contract grant number: NSC95-2622-E-238-019-CC3.

from solution,[13] *in situ* intercalative polymerization,[14] and melt intercalation.[15]

Much effort has previously been exerted for the preparation and characterization of PLA/laminar silicate nanocomposites and for the determination of the influence of the crystallization conditions, including the crystallization temperature, crystallization time, crystallization rate, and concentration of the nucleating agent, on the resulting morphology.[16–28] In contrast, less attention has been focused on investigating the intermolecular interactions that exist between PLA and the clay under various isothermal crystallization conditions.

In this study, we employed a solution intercalation technique to prepare nanocomposites from PLLA and an organophilic MMT. After crystallizing the PLLA/MMT nanocomposites at various isothermal crystallization temperatures, we investigated the distribution of MMT in the matrix, the melting and crystallization conditions of the PLLA/MMT nanocomposites, and their morphologies and crystallinities. Moreover, we determined the effect of the isothermal crystallization temperature on the intermolecular interactions of the PLLA/MMT nanocomposites.

EXPERIMENTAL

Materials

PLLA (molecular weight = 85,000–160,000 g/mol) was purchased from Sigma (St. Louis, MO). The sodium cation of MMT clay (PK805) was purchased from Paikong (Taipei, Taiwan). Dilauryl dimethyl ammonium bromide {DDAB or $[CH_3(CH_2)_{11}]_2(CH_3)_2NBr$} was purchased from TCI (Tokyo, Japan). THF was obtained from Tedia (Fairfield, OH).

Preparation of organophilic MMT

The MMT powder (5 g) was suspended in an aqueous solution of DDAB and agitated for 24 h at room temperature. The resulting modified clay was filtered and then washed repeatedly with distilled water until no light yellow AgBr precipitate was observed during titration of the filtrate with $AgNO_3$; this ensured that no Br^- ions existed in solution. The wet, modified clay was dried in a vacuum oven at 100°C. The dried, modified clay was then ground into a powder and passed through a 325-mesh sieve. The particle diameter of the resulting powder was about 40 μm.

Preparation of the PLLA/MMT nanocomposites

The organophilic MMT was mixed at various ratios (2–8 wt %) with PLLA (1 g) in THF (10 mL) and then stirred at 60°C for 24 h. The solution was then cast into film form and dried in a vacuum oven.

Preparation of isothermally crystallized specimens

The sample was placed on a hot plate and heated to 190°C. This temperature was maintained for at least 3 min to thoroughly melt the specimen, which was then quickly transferred to an oven and crystallized for 12 h at an isothermal crystallization temperature of 100, 110, 120, 130, 140, 150, 160, or 170°C.

Characterization

Wide-angle X-ray diffraction

A Thermo ARL X'tra X-ray diffractometer (Waltham, MA) was used to obtain the X-ray diffraction (XRD) patterns of the samples. The X-ray beam was Ni-filtered Cu Kα radiation from a sealed tube. To calculate the *d*-spacing, Bragg's law was used:

$$n\lambda = 2d \sin\theta$$

where θ is the angle between the incident ray and the scattering planes, *n* is an integer determined by the order given, and λ is the wavelength. The organophilic MMT and the PLLA/MMT nanocomposites were analyzed within the 2θ range of 1–25°; the scanning rate was 1.5°/min.

Transmission electron microscopy (TEM)

The samples for TEM analysis were prepared by the placement of films of the PLLA/MMT nanocomposites into epoxy resin capsules and by the curing of the epoxy resin at 70°C for 24 h in a vacuum oven. Then, the cured epoxy resin containing the PLLA/MMT nanocomposite was microtomed with a Reichert–Jung Ultracut-E into 60–90-nm-thick slices (Optische Werke AG Wien, Austria). Subsequently, one layer of carbon (ca. 10 nm thick) was deposited onto these slices on 100-mesh copper nets for TEM observation with a JEOL 2010 instrument (Tokyo, Japan) operated at an acceleration voltage of 200 kV.

Polarizing optical microscopy (POM)

A Leitz Labor Lux 12 POLS polarizing optical microscope (Bannockburn, IL) equipped with a charged coupling device detector was operated at a magnification of 125× to observe the crystallization modes of the PLLA/MMT nanocomposites. The sample temperature was increased from room temperature to 190°C with a controlled heater. This temperature was then maintained for 2 min to ensure that the sample had melted completely. The sample was then cooled to a temperature within the range of 120–170°C.

Differential scanning calorimetry (DSC)

A PerkinElmer series 6 differential scanning calorimeter was used to examine the melting and

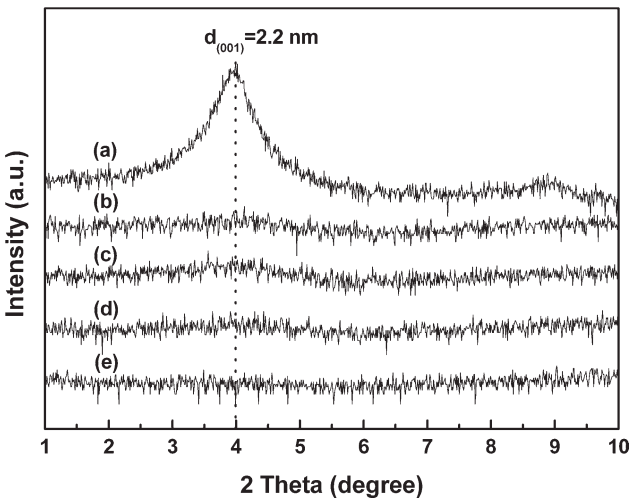

Figure 1 XRD spectra of (a) MMT and (b–e) PLLA/MMT nanocomposites incorporating 2, 3, 4, and 5 wt % MMT, respectively.

crystallization behavior of the samples. The crystallinity was calculated with the following equation:

$$\text{Crystallinity } (\%) = 100 \times \frac{\Delta H_f}{f \Delta H_f^{\infty}}$$

where ΔH_f is the heat of fusion, ΔH_f^{∞} is the heat of fusion of ideally crystalline PLLA (94 J/g), and f is the weight fraction (in these experiments, f was equal to 1). The DSC experiment was performed with an N_2 flow rate of 20 mL/min. The procedure comprised six stages:

1. Isothermal: The aluminum plate was placed in the DSC instrument for 1 min at 25°C to ensure temperature stability.
2. Temperature scan: The sample was heated from 25 to 190°C at a rate of 20°C/min.
3. Isothermal: The temperature was maintained at 190°C for 2 min to eliminate the thermal history.
4. Temperature scan: The sample was cooled from 190 to 25°C at a rate of 2°C/min.
5. Isothermal: The temperature was maintained at 25°C for 1 min to ensure temperature stability.
6. Temperature scan: The sample was heated from 25 to 190°C at a rate of 2°C/min.

Thermogravimetric analysis (TGA)

TGA of the PLLA and PLLA/MMT nanocomposites was accomplished with a PerkinElmer TGA-7 instrument. In all tests, the samples were heated under N_2 from 25 to 450°C at a heating rate of 10°C/min.

Raman spectroscopy

A Renishaw inVia Raman microscope was used to study the molecular interactions within the samples. The wavelength of the light source was 785 nm. A silicon chip (520 cm^{-1}) was employed to calibrate the instrument before sample measurement. The instrument's tolerance was controlled within ± 1 cm^{-1}.

Fourier transform infrared (FTIR) spectroscopy

A PerkinElmer Spectrum One FTIR spectrometer (scan range = 4000–650 cm^{-1}) was employed to study the molecular interactions within the samples.

RESULTS AND DISCUSSION

PLLA/MMT nanocomposites

We used XRD to determine the distribution of MMT in PLLA. Figure 1 displays the XRD spectra of MMT and a series of PLLA/MMT nanocomposites. The 2θ diffraction peak for the $d_{(001)}$ facet of MMT appeared at 4°, and this revealed that the laminate distance was 2.2 nm. After PLLA had been added, the $d_{(001)}$ signal was no longer visible, and this suggested that the distance between the MMT layers had expanded dramatically; that is, its layer structure was totally destroyed, and this resulted in an even distribution within the PLLA matrix.

Figure 2 displays the XRD spectra of pure PLLA and PLLA samples incorporating various quantities of MMT. The signal for the 200/110 facet of crystalline PLLA moved slightly to the left (from 16.6 to 16.4°) when the quantity of the clay was increased to 5 wt %, and the shape of the signals in the XRD spectra of the PLLA/MMT samples was similar to that of pure PLLA. Therefore, it appears that

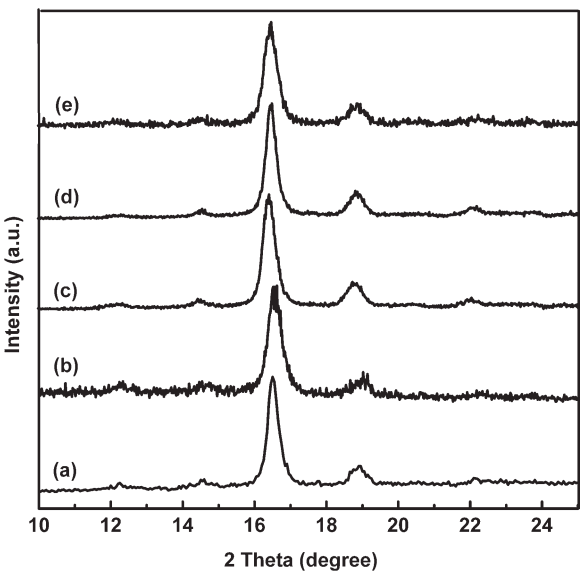

Figure 2 XRD spectra of PLLA/MMT nanocomposites incorporating (a) 0, (b) 2, (c) 3, (d) 4, and (e) 5 wt % MMT.

Figure 3 TEM micrograph (25,000×) of the PLLA/MMT nanocomposite incorporating 5 wt % MMT.

spreading MMT into the PLLA matrix had little impact on the crystallite structure.

Figure 3 displays a TEM micrograph of a cross section of the PLLA/MMT nanocomposite incorporating 5 wt % MMT. At 25,000× magnification, the MMT units appeared to be evenly distributed within the PLLA.

These results revealed that the organophilic MMT platelets (2, 3, 4, or 5 wt %) were always exfoliated within the PLLA polymer matrix, which retained its crystallite structure.[29–31]

Morphology of the isothermally crystallized nanocomposites

It is possible to obtain PLLA nanocomposites with a specific morphology (e.g., single crystals, spherical crystals, or dendrites) through changes in the crystallization conditions. In this study, upon cooling, the crystallite aggregates grew in the form of spherulites; the nuclei on the heterogeneous cores gradually grew along the radiant direction until they came into contact with adjacent spherulites.[32]

Using POM to observe the isothermal crystallization of PLLA/MMT nanocomposites incorporating 2 wt % MMT, we found that the spherulite model varied with the temperature (Fig. 4). At 120°C, nucleation was rapid, and many small and randomly oriented crystals were formed. At 130°C, the spherulites possessed a Maltese cross pattern.[33] When the temperature increased, the rate of nucleation decreased; this reduced the number of nuclei and thereby facilitated crystallite growth in all directions. As a result, at 150°C, crystallization occurred in a radiant spreading mode, and dendrites were formed. At 160 and 170°C, ringed spherulites formed. According to Figure 4, the spherulite size was directly proportional to the crystallization temperature.

XRD analysis

Figure 5 displays XRD patterns of PLLA/MMT nanocomposites incorporating organophilic MMT (2 wt %) that were subjected to isothermal crystallization at various temperatures. Isothermal crystallization of these PLLA/MMT nanocomposites at 100, 110, 120, and 130°C resulted in stronger diffraction peaks for the 200/110 and 203 crystal facets than those obtained at higher isothermal crystallization temperatures, presumably because of the presence of more Maltese cross-patterned crystals. Moreover, three additional diffraction peaks appeared for the

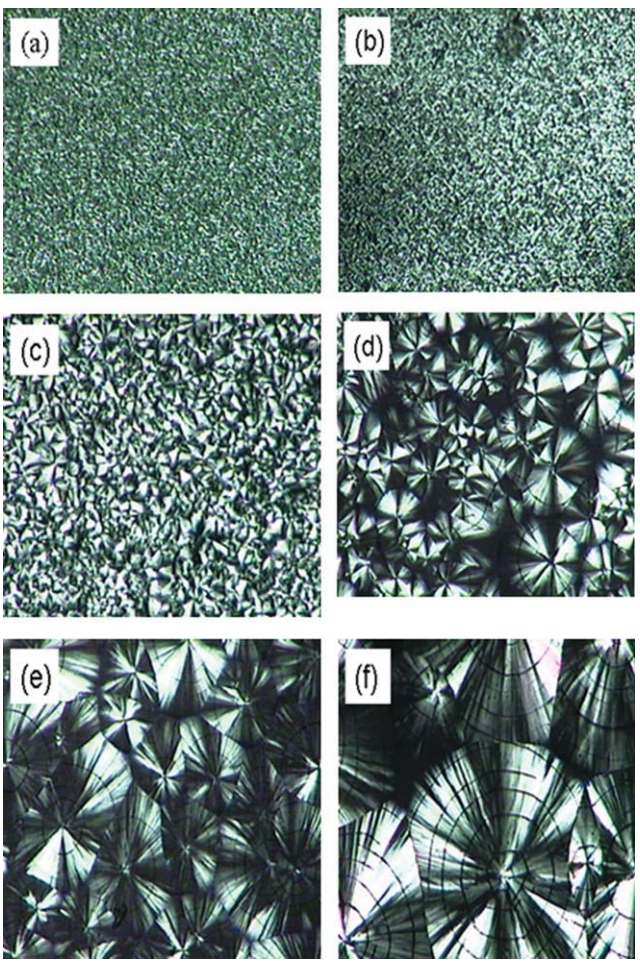

Figure 4 Crystallization modes of PLLA/2 wt % MMT nanocomposites prepared by isothermal crystallization at (a) 120, (b) 130, (c) 140, (d) 150, (e) 160, and (f) 170°C (original magnification = 125×). [Color figure can be viewed in the online issue, which is available at www.interscience.wiley.com.]

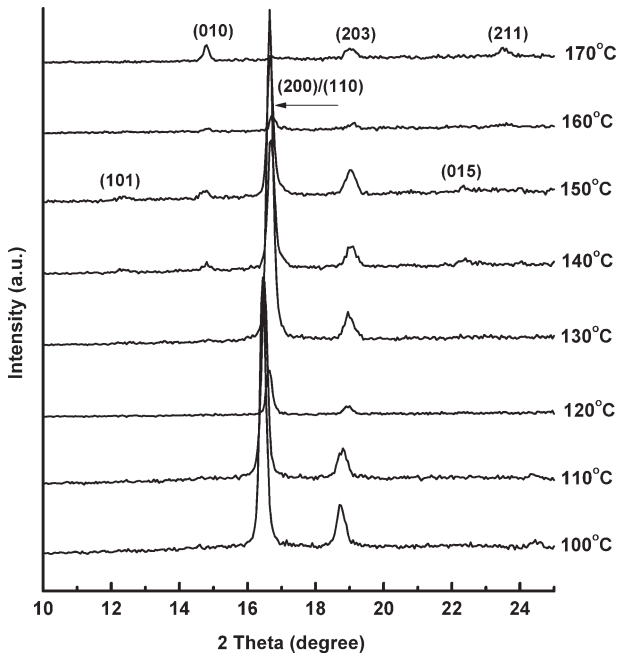

Figure 5 XRD spectra of PLLA/2 wt % MMT nanocomposites prepared at various isothermal crystallization temperatures.

015, 101, and 010 facets for the samples prepared at 140 and 150°C; that is, these samples crystallized in different conformations with respect to those of the lower temperature treated samples. Subsequently, the intensities of the absorptions of the 200/110 and 203 crystal facets decreased dramatically as the crystallization temperature increased to 160 and 170°C, presumably because ringed spherulites, rather than Maltese cross-patterned crystals, formed at higher crystallization temperatures. The results are consistent with those obtained with POM to investigate the morphology of the PLLA/MMT nanocomposites. Table I summarizes the XRD peaks of these PLLA/MMT nanocomposites; Table II lists the corresponding intensities. We conclude that the isothermal crystallization temperature employed for the formation of the PLLA/MMT nanocomposites affected both the spherulite model and size.

TABLE II
Intensities of the XRD Peaks of the PLLA/2 wt% MMT Nanocomposites Prepared at Various Crystallization Temperatures

Crystallization temperature (°C)	Intensity					
	101	010	200/110	203	015	211
100	—	—	1176.5	249.5	—	—
110	—	—	956	183.5	—	—
120	—	—	216.5	51	—	—
130	—		1560.5	160.5	—	—
140	32.5	64.5	627	132	82	—
150	40.5	66.5	681	162	90.5	—
160	—	25.5	84.5	53	—	—
170	—	84.5	36	69	—	72

DSC analysis

DSC involves the heating (or cooling) of a test sample together with a thermally inert material at a constant rate of heating (or cooling). Any temperature difference between the test sample and the reference arises from endothermic or exothermic reactions of the test sample, such as phase changes, melting, or structural changes within crystals. In general, phase changes are endothermic, and crystallization reactions are exothermic. We employed DSC analysis to determine the changes in T_m and the degrees of crystallinity of our samples.

Figure 6 displays cooling curves for the PLLA/2 wt % MMT nanocomposites prepared at various isothermal crystallization temperatures. The crystallization temperature of these PLLA/MMT nanocomposites increased (from 124.6 to 137.6°C), and the peak became sharper as the isothermal crystallization temperature increased, presumably because the crystallite structures possessed a more perfect and uniform size at higher isothermal crystallization temperatures.

Figure 7 presents the heating curves of PLLA/2 wt % MMT nanocomposites subjected to isothermal crystallization at various temperatures. We can observe two endothermic peaks in the curves of the samples prepared through isothermal crystallization at 100, 110, 120, 130, and 140°C but only one for the

TABLE I
Values of 2θ for the PLLA/2 wt% MMT Nanocomposites Prepared at Various Crystallization Temperatures

Crystallization temperature (°C)	2θ (°)					
	hkl = 101	*hkl* = 010	*hkl* = 200/110	*hkl* = 203	*hkl* = 015	2 *hkl* = 11
100	—	—	16.4	18.7	—	—
110	—	—	16.5	18.8	—	—
120	—	—	16.6	19.0	—	—
130	—	14.9	16.7	19.0	—	—
140	12.3	15.0	16.7	19.1	22.4	—
150	12.6	14.8	16.7	19.1	22.4	—
160	—	14.9	16.7	19.2	—	—
170	—	14.8	16.7	19.1	—	23.5

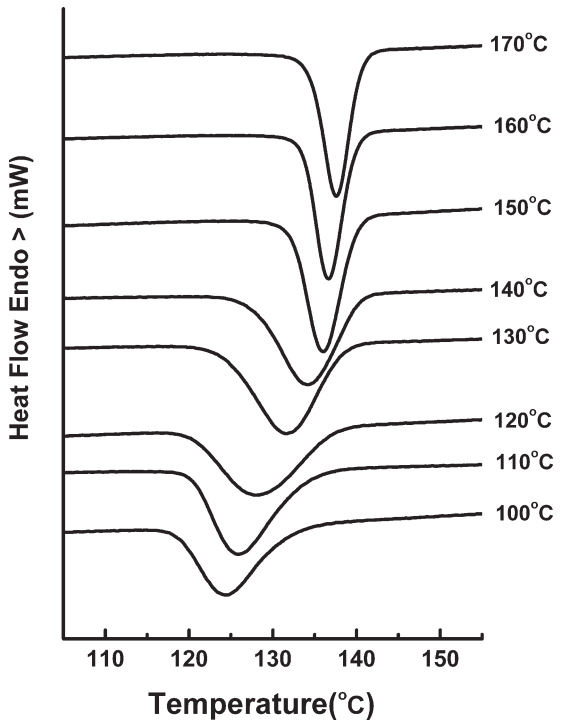

Figure 6 DSC thermograms (cooling scan) of PLLA/2 wt % MMT nanocomposites prepared at various crystallization temperatures (scan range = 25–190°C, scan rate = 2°C/min).

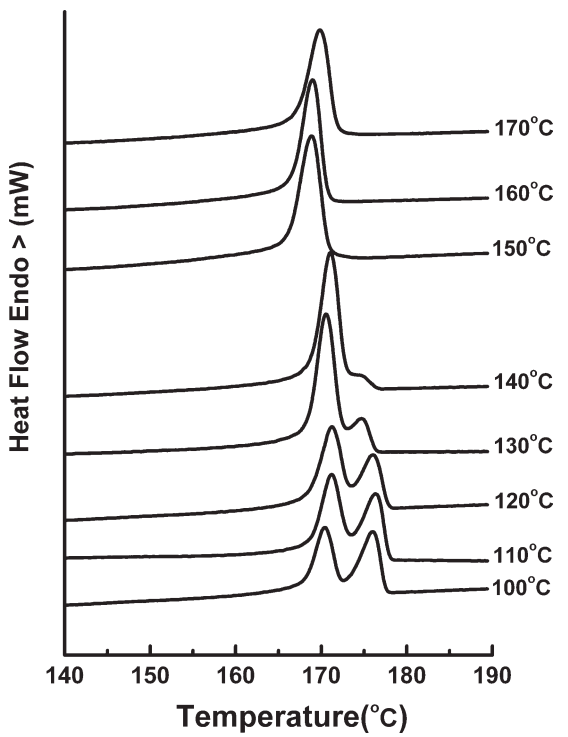

Figure 7 DSC thermograms (second heating scan) of PLLA/2 wt % MMT nanocomposites prepared at various crystallization temperatures (scan range = 25–190°C, scan rate = 2°C/min).

TABLE III
Crystallinities and Total Enthalpies of the Test Samples Prepared at Various Isothermal Crystallization Temperatures

Crystallization temperature (°C)	T_c (°C)	ΔH_c (J/g)	T_1 (°C)	T_2 (°C)	ΔH_f (J/g)	X_c (%)
Untreated	121.3	−42.0	168.1	174.8	52.6	56.0
100	124.6	−41.5	170.4	176.0	43.6	46.4
110	125.8	−42.3	171.2	176.4	44.6	47.4
120	128.1	−46.2	171.3	176.1	46.9	49.9
130	131.6	−47.5	170.5	174.7	51.8	55.1
140	134.3	−43.6	171.0	174.9	45.9	48.8
150	136.1	−45.6	168.9	—	47.2	50.2
160	136.7	−45.3	168.9	—	48.5	51.6
170	137.6	−46.2	169.8	—	46.8	49.8

T_1 = endothermic peak 1; T_2 = endothermic peak 2; T_c = crystallization temperature; ΔH_c = enthalpy of crystallization; X_c = degree of crystallization.

samples obtained at 150, 160, and 170°C. The presence of a higher temperature endothermic peak indicates that recrystallization of the melted crystal occurred to form a more stable crystal, which underwent fusion again when the heating temperature of the DSC instrument was increased. The phenomenon of recrystallization occurred at lower isothermal crystallization temperatures.

Table III lists the crystallization temperatures, endothermic peaks, enthalpies of fusion and crystallization, and degrees of crystallinity of the PLLA/2 wt % MMT nanocomposites prepared under various isothermal crystallization conditions. Figure 8 displays the variation in the degree of crystallization of the test samples with respect to the isothermal crystallization temperature. The plot is irregular, presumably because the degree of crystal formation, which proceeds through nucleation and growth steps, is related to the crystallization temperature; the optimal crystallization temperature was 130°C.

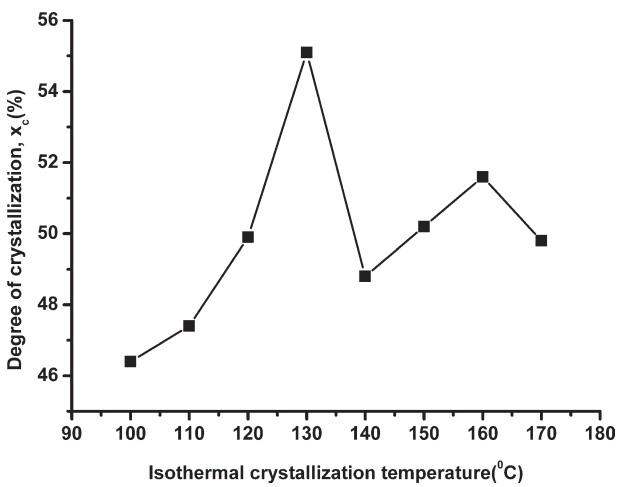

Figure 8 Variations in the degrees of crystallization of the test samples prepared at various isothermal crystallization temperatures.

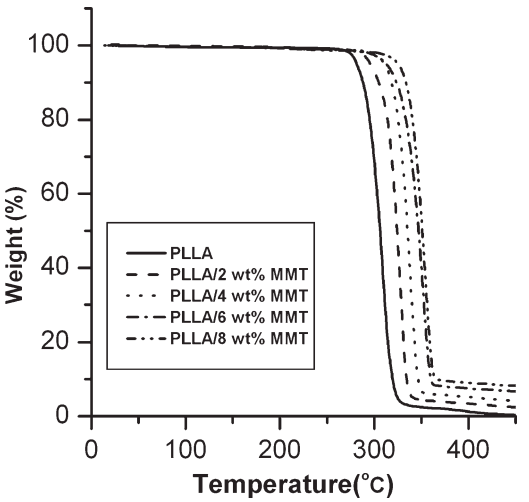

Figure 9 TGA heating curves of PLLA/MMT nanocomposites (heating range = 25–450°C, heating rate = 10°C/min).

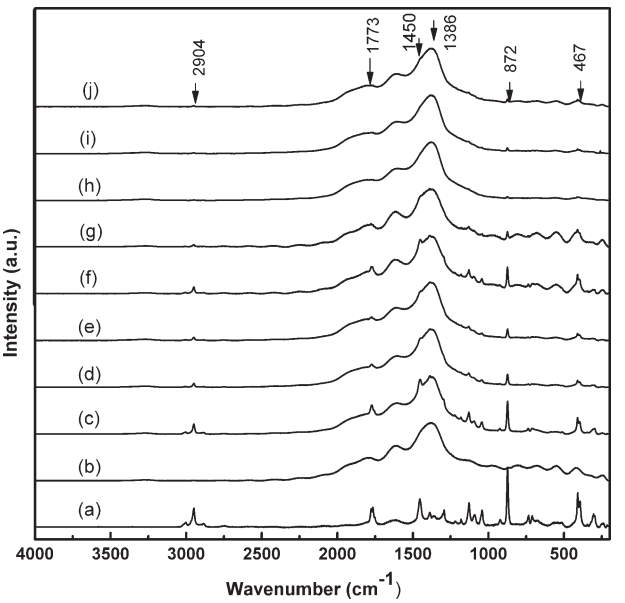

Figure 10 Raman spectra of PLLA/2 wt % MMT nanocomposites prepared at various crystallization temperatures: (a) untreated; (b) melt-quenched; and (c) 100, (d) 110, (e) 120, (f) 130, (g) 140, (h) 150, (i) 160, and (j) 170°C.

Thermal stability

Figure 9 displays TGA thermograms of the PLLA/MMT nanocomposites and the parent polymer, PLLA. The nanocomposites exhibited superior thermal stability with respect to that of the parent polymer. The decomposition temperatures of the PLLA/MMT nanocomposites were all greater than 250°C. Table IV lists the temperature at which 5% weight loss occurred ($T_{5\%}$), the temperature at which the polymer's maximum rate of weight loss occurred (T_{max}), and the residue remaining (char yield) at 400°C for the PLLA/MMT systems. The values of $T_{5\%}$ and T_{max} of the nanocomposites increased as the content of organophilic MMT increased, and this suggested enhanced interactions between the clay nanolayers and PLLA, which also reinforced the decomposition temperatures of the PLLA/MMT nanocomposites. As expected, the char yield at 400°C increased as the amount of organophilic MMT increased in the PLLA/MMT nanocomposites.

Intermolecular interactions

Raman and FTIR spectra can be used to detect changes in the vibratory energy levels of molecules. Because these two spectroscopic methods are mutually complementary, they allow the vibration peaks of molecules to be determined comprehensively.

Figure 10 displays Raman spectra of the PLLA/2 wt % MMT nanocomposites prepared under various isothermal crystallization conditions. The absorption peaks obtained when the isothermal crystallization temperatures were low (100–140°C) were more complex than those obtained at higher temperatures (150–170°C); for example, signals at 2904, 1773, 1450, 872, and 467 cm^{-1} appeared only at lower isothermal crystallization temperatures.

FTIR spectroscopy allowed us to determine the causes of the variations in specific functions and the changes in the intermolecular interactions of the various PLLA/MMT nanocomposites (Figs. 11–14). A boundary appears to exist at 130–140°C, with the shape or position of the absorption peaks being significantly different when the isothermal crystallization temperature was above or below these temperatures. For example, the absorption peak of the C=O groups of the PLLA/MMT nanocomposites split into two signals at 1748 and 1755 cm^{-1} when the isothermal crystallization temperature was increased to 140°C (Fig. 12). Furthermore, the absorption peak for the $\delta_{as}(CH_3)$ and $\delta_s(CH_3)$ deformations of the PLLA/MMT nanocomposites split into two signals at 1305 and 1293 cm^{-1} when the isothermal crystallization temperature was higher than 140°C; it was a broad peak when the isothermal crystallization temperature was below 130°C (Fig. 13). The intensities of the signals at 736, 712, 693, and 686 cm^{-1} for the $\nu_{as}(CH_3)$ and $\nu_s(CH_3)$ deformations of the PLLA/MMT nanocomposites all increased significantly as the isothermal crystallization temperature increased (Fig. 14). In addition, the intensity of the signal at 1209 cm^{-1} for asymmetric C—O—C stretching increased dramatically

TABLE IV
TGA Data for PLLA and the PLLA/MMT Nanocomposites

MMT content (%)	0	2	4	6	8
$T_{5\%}$ (°C)	281	296	310	313	325
T_{max} (°C)	306	324	335	347	351
Char yield at 400°C (%)	1.3	3.4	5.3	7.7	9.0

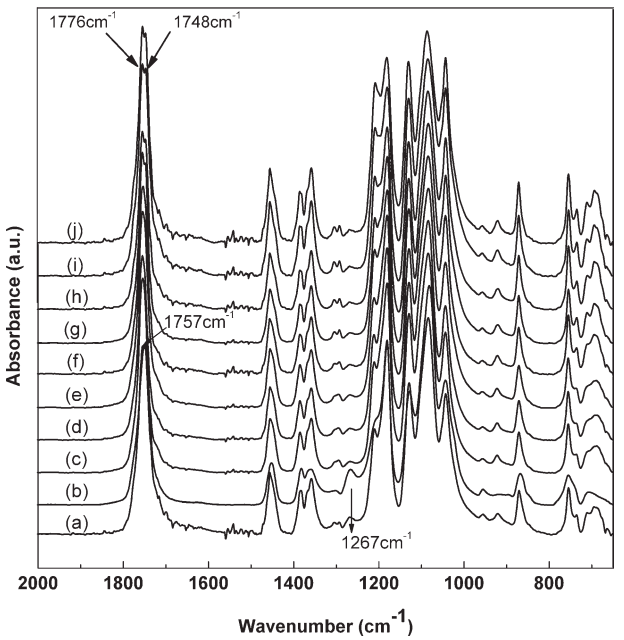

Figure 11 FTIR spectra of PLLA/2 wt % MMT nanocomposites prepared at various crystallization temperatures: (a) untreated; (b) melt-quenched; and (c) 100, (d) 110, (e) 120, (f) 130, (g) 140, (h) 150, (i) 160, and (j) 170°C.

when the isothermal crystallization temperature increased. Table V summarizes the differences in the appearances of the absorption peaks in the Raman and FTIR spectra of the samples prepared at the various isothermal crystallization temperatures.

The results indicate that there were marked differences in the intermolecular interactions of the

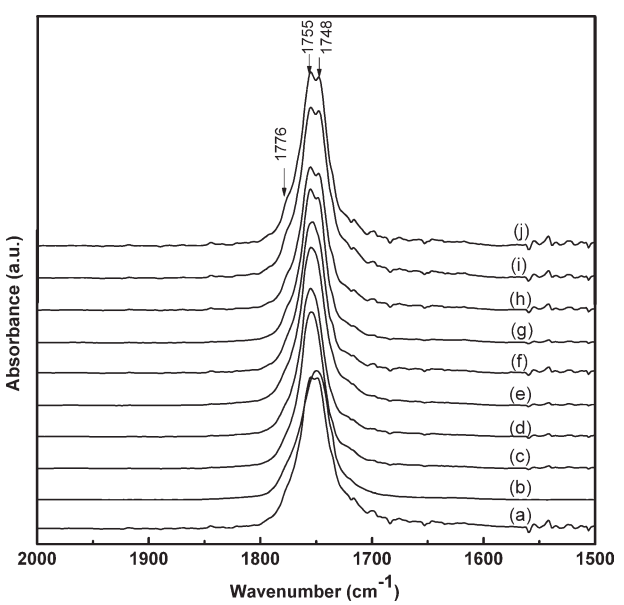

Figure 12 FTIR spectra (C=O stretching region) of PLLA/2 wt % MMT nanocomposites prepared at various isothermal crystallization temperatures: (a) untreated; (b) melt-quenched; and (c) 100, (d) 110, (e) 120, (f) 130, (g) 140, (h) 150, (i) 160, and (j) 170°C.

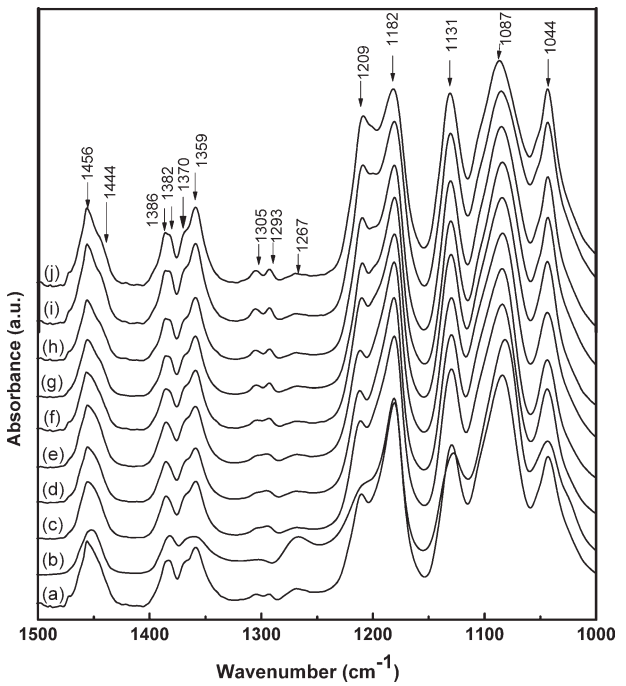

Figure 13 FTIR spectra [$\delta_{as}(CH_3)$ and $\delta_s(CH_3)$ deformation bands] of PLLA/2 wt % MMT nanocomposites prepared at various isothermal crystallization temperatures: (a) untreated; (b) melt-quenched; and (c) 100, (d) 110, (e) 120, (f) 130, (g) 140, (h) 150, (i) 160, and (j) 170°C.

PLLA/MMT nanocomposites between the isothermal crystallization temperature below and the boundary temperature above. We assumed that the different conformations of the PLLA/MMT nanocomposites within different ranges of isothermal crystallization temperatures were a major cause of the different intermolecular interactions (e.g., the

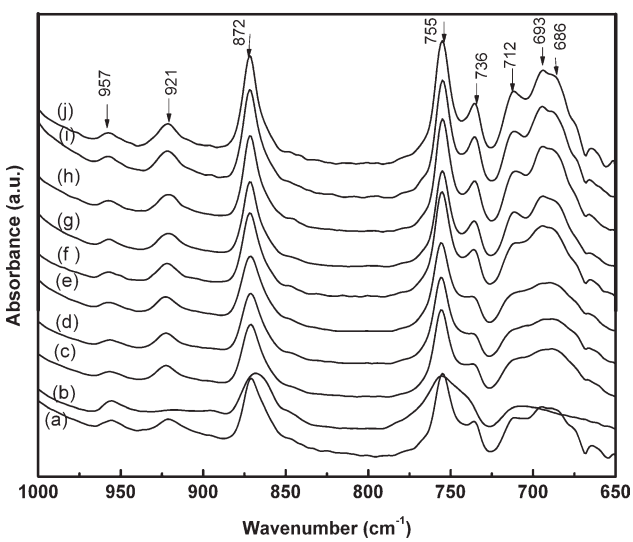

Figure 14 FTIR spectra [$\nu_{as}(CH_3)$ and $\nu_s(CH_3)$ deformation bands] of PLLA/2 wt % MMT nanocomposites prepared at various isothermal crystallization temperatures: (a) untreated; (b) melt-quenched; and (c) 100, (d) 110, (e) 120, (f) 130, (g) 140, (h) 150, (i) 160, and (j) 170°C.

TABLE V
Shapes of the Absorption Peaks in the Raman and FTIR Spectra of the PLLA/MMT Nanocomposites Prepared at Various Isothermal Crystallization Temperatures

	Raman					FTIR			
Crystallization temperature (°C)	2900 cm^{-1}	1773 cm^{-1}	1450 cm^{-1}	872 cm^{-1}	450 cm^{-1}	1755–1748 cm^{-1}	1305–1293 cm^{-1}	736 cm^{-1}	712–693–686 cm^{-1}
100	∨	∨	∨	∨	∨	∨	○	△	○
110	∨	∨	∨	∨	∨	∨	○	△	○
120	∨	∨	∨	∨	∨	∨	○	△	○
130	∨	∨	∨	∨	∨	∨	★	∨	△
140	△	△	△	∨	∨	★	★	∨	★
150	—	○	—	—	—	★	★	∨	★
160	—	○	—	—	—	★	★	∨	★
170	—	○	—	—	—	★	★	∨	★

★ = split peak; ∨ = peak; △ = no obvious peak; — = no peak; ○ = broad peak.

extent of London dispersion forces and the extent of dipole-induced dipole forces) of the PLLA/MMT nanocomposites. In the POM, XRD, and DSC analyses, a boundary temperature (130 or 140°C) also existed that led to two different results.

CONCLUSIONS

Organophilic MMT became exfoliated when it was placed within a PLLA polymer matrix, but the crystallite construction of PLLA was retained. POM and XRD analyses of these PLLA/MMT nanocomposites, which were prepared under isothermal crystallization conditions, indicated that the crystal modes and structures varied and the crystal sizes increased as the isothermal crystallization temperature increased. The PLLA nanocomposites incorporating organophilic MMT exhibited different crystal facets when they were prepared at different crystallization temperatures; that is, the spherulite model changed. Maltese cross patterns existed after isothermal crystallization at lower temperatures; ringed spherulites formed at higher temperatures. DSC analysis revealed the presence of the phenomenon of recrystallization at lower isothermal crystallization temperatures (100–140°C). In addition, the crystallization temperature of these PLLA/MMT nanocomposites increased (from 124.6 to 137.6°C), and this revealed that the crystalline structure was more perfect when the isothermal crystallization temperature was increased. TGA revealed an effective enhancement of the thermal stability as the amount of organophilic MMT increased in the PLLA/MMT nanocomposites. Raman and FTIR spectra revealed that the conformations of the PLLA/MMT nanocomposites prepared at the various isothermal crystallization temperatures affected their modes of intermolecular interaction.

References

1. Ray, S. S.; Bousmina, M. Prog Mater Sci 2005, 50, 962.
2. Gorrasi, G.; Tortora, M.; Vittoria, V. J Polym Sci Part B: Polym Phys 2005, 43, 2454.
3. Ni, P.; Li, J.; Suo, J.; Li, S. J Appl Polym Sci 2004, 94, 534.
4. Goda, H.; Frank, C. W. Chem Mater 2001, 13, 2783.
5. Chang, J. H.; An, Y. U. J Polym Sci Part B: Polym Phys 2002, 40, 670.
6. Lee, M. H.; Dan, C. H.; Kim, J. H.; Cha, J.; Kim, S.; Hwang, Y.; Lee, C. H. Polymer 2006, 47, 4359.
7. Weon, J. I.; Sue, H. J. Polymer 2005, 46, 6325.
8. Xu, Y.; Hoa, S. V. Compos Sci Technol 2008, 68, 854.
9. Balakrishnan, S.; Start, P. R.; Raghavan, D.; Hudson, S. D. Polymer 2005, 46, 11255.
10. Agag, T.; Koga, T.; Takeichi, T. Polymer 2001, 42, 3399.
11. Delozier, D. M.; Orwoll, R. A.; Cahoon, J. F.; Johnston, N. J.; Smith, J. G.; Connell, J. W. Polymer 2002, 43, 813.
12. Park, C.; Smith, J. G.; Connell, J. W.; Lowther, S. E.; Working, D. C. Polymer 2005, 46, 9694.
13. Yano, K.; Usuki, A.; Okada, A.; Kurauchi, T.; Kamigaito, O. Polym Prepr (Jpn) 1991, 32, 65.
14. Kojima, Y.; Usuki, A.; Kawasumi, M.; Fukushima, Y.; Okada, A.; Kurauchi, T.; Kamigaito, O. J Mater Res 1993, 8, 1179.
15. Vaia, R. A.; Giannelis, E. P. Macromolecules 1997, 30, 7990.
16. Pluta, M. Polymer 2004, 45, 8239.
17. Ray, S. S.; Yamada, K.; Ogami, A.; Okamoto, M.; Ueda, K. Macromol Rapid Commun 2002, 23, 943.
18. Ray, S. S.; Maiti, P.; Okamoto, M.; Yamada, K.; Ueda, K. Macromolecules 2002, 35, 3104.
19. Krikorian, V.; Pochan, D. J. Chem Mater 2003, 15, 4317.
20. Ray, S. S.; Okamoto, M. Macromol Rapid Commun 2003, 24, 815.
21. Ray, S. S.; Okamoto, M. Macromol Mater Eng 2003, 288, 936.
22. Ray, S. S.; Yamada, K.; Okamoto, M.; Ogami, A.; Ueda, K. Chem Mater 2003, 15, 1456.
23. Ray, S. S.; Yamada, K.; Okamoto, M.; Ueda, K. Polymer 2003, 44, 857.
24. Hiroi, R.; Ray, S. S.; Okamoto, M.; Shiroi, T. Macromol Rapid Commun 2004, 25, 1359.
25. Krikorian, V.; Pochan, D. J. Macromolecules 2004, 37, 6480.
26. Di, Y.; Iannace, S.; Maio, E. D.; Nicolais, L. J Polym Sci Part B: Polym Phys 2005, 43, 689.
27. Wu, T.; Chiang, M. Polym Eng Sci 2005, 45, 1615.
28. Pluta, M.; Paul, M.; Alexandre, M.; Dubois, P. J Polym Sci Part B: Polym Phys 2006, 44, 312.
29. Navarchian, A. H.; Majdzadeh-Ardakani, K. J Appl Polym Sci 2009, 114, 531.
30. Ozkoc, G.; Kemaloglu, S. J Appl Polym Sci 2009, 114, 2481.
31. Miyagawa, H.; Rich, M. J.; Drzal, L. T. J Polym Sci Part B: Polym Phys 2004, 42, 4384.
32. Fried, J. R. Polymer Science and Technology, 2nd ed.; Prentice Hall PTR: Upper Saddle River, NJ, 2003; p 158.
33. Bower, D. J. An Introduction to Polymer Physics; Cambridge University Press: Cambridge, England, 2002; p 117.